Two-Dimensional Air Exfiltration and Heat Transfer Through Fiberglass Insulation I. Numerical Model and Experimental Facility

Hong Chen **Robert W. Besant, P.E.** Fellow ASHRAE **Yong-Xin Tao, Ph.D.** Member ASHRAE

A numerical model, employing a local-averaging formulation, was developed for heat transfer and water vapor deposition within fiberglass insulation under air exfiltration and frosting conditions. Frost growth on the cold surface was modeled using special frost growth boundary conditions. Non-isotropic permeability effects that occur in fiberglass boards were included in the model for porous medium flow because tests showed that the permeability for flow parallel to the plane of the boards was 69% higher than perpendicular to the insulation boards. Transient heat and moisture transfer processes within a thick layer of fiberglass insulation were modeled for steady exfiltration of humid air (60% to 84% rh) with a two-dimensional airflow during winter temperature conditions. In order to validate the numerical model, laboratory apparatus was constructed with a test cell 135 mm high, 600 mm wide and 275 mm deep. This allowed a two-dimensional moist air exfiltration [0.5 to 1.5 L/(m^2·s)] through a fiberglass insulation slab for a temperature range −20°C to 21.5°C from the cold outside surface to the warm inside surface. Using this apparatus, the transient temperature profiles, moisture accumulation profiles, and heat-flux at the cold side of the fiber-glass insulation were measured during the air exfiltration process. Part I outlines the theoretical/numerical model and describes the experimental test facilities and the properties of the fiberglass insulation tested. Part II of this paper presents the comparisons of experimental data and corresponding simulation results.

INTRODUCTION

In recent years, many studies have been done on building envelopes and on the vapor retarders and insulation materials used to reduce moisture deposition and heat transfer. For example, Paljak (1973), Tobiasson et al. (1979), Langlais et al. (1983), Thomas et al. (1983), Bomberg et al. (1978, 1991), Pedersen (1990) and Pedersen et al. (1991) showed that heat flow within insulation depends on the type of insulation, its moisture content, and the temperature of the insulation. A comprehensive review of moisture effects in insulation materials is provided in the book edited by Trechsel (1994), while recent papers on insulation materials are presented in the book edited by Graves and Wysocki (1991), the proceedings of CIB meetings (1993) and (1995), and the final report of IEA Annex 24 (1996).

Moisture accumulation may alter the heat flow in both sensible and latent forms. In sensible forms, the presence of the liquid and frost phases results in an increase in the thermal conductivity of the insulation while the release of latent heat may alter the temperature profiles and heat flux. Energy transfer increases of about 3 to 5% for each percent increase in moisture content by volume were shown by Epstein et al. (1977) and Larsson et al. (1977). On the other hand, Hedlin (1983) showed that roof structures with less than 2% moisture content could double the heat rate

Hong Chen is a graduate student and **Robert W. Besant** a professor in the Department of Mechanical Engineering, University of Saskatchewan, Canada. **Yong-Xin Tao** is an assistant professor in the Mechanical Engineering Department, Tennessee State University, Nashville.

with typical diurnal cycles in temperature. Furthermore, the moisture within the insulation can lead to mold growth, degradation of some organic materials, rust damage to some metallic components, and freezing damage in the condensation zone at low temperature (Lstiburek and Carmody 1990). Therefore, it is crucial to study the conditions which cause the moisture accumulation and water vapor transport within insulation material. In cold climate countries, the most severe moisture problem occurs in winter (Kumaran 1992) where the operating temperature of thermal insulation is below freezing.

For several decades, research work has been done on the numerical modeling of heat and moisture deposition and the movement of water vapor within porous insulating materials used in building envelopes. A large number of papers have been written on this topic. For example,: Vafai and Saker (1986) have studied the condensation effect within the fibrous insulation; Kohonen and Ojanen (1987) predicted hygrothermal effects of combined natural/forced convection in 2-D at a non-steady-state condition, Tien and Vafai (1990) numerically studied the effects of air infiltration on the moisture distribution within an isotropic insulation matrix. In addition, Murata (1995) studied the heat and mass transfer with condensation in fibrous insulation slab bounded on one side by a cold surface, Ojanen and Simonson (1995) experimentally and numerically investigated forced convection past various insulated wall structures, and Pierce and Benner (1986) investigated thermally induced hygroscopic mass transfer for a closed system of insulation.

Some recent authors have written a number of papers presenting both experimental data and numerical simulations of heat and water vapor transfer with moisture and frost accumulation: Tao et al. (1991a, 1991b, 1992, 1993), Simonson et al. (1993) and Mitchell et al. (1995). Frost growth within porous insulation has been shown to alter substantially the heat flux and mass of water accumulation within fiberglass.

This study extends the work of Mitchell et al. (1995) for one-dimensional air exfiltration through an insulation slab to one with more realistic boundary and flow conditions and frost accumulation on a cold surface (simulating an exterior envelope surface) for a cavity completely filled with insulation. The main objective of this study was to develop an accurate numerical model for the complex physical processes that occur within various porous insulation materials like fiberglass which undergo heat transfer and air exfiltration with moisture and frost accumulation.

Part I presents the numerical model and the test facilities that were used to collect data that can be used to compare with the simulation results. These comparisons are in Part II.

NUMERICAL MODEL

A schematic, detailing the geometry for the numerical model, is presented in Figure 1. The solution domain of the numerical model was a two-dimensional rectangular porous medium (fiberglass insulation). Air was introduced at a line source at the top left corner (point A in Figure 1) for air exfiltration, while a line sink removed this airflow at point B. Experimentally, the line sink and source are slots of height h such that $h/b = 0.04$. The boundary conditions were uniform sub-freezing temperature T_c on the cold bottom side and uniform room temperature T_h on the warm top side. The right and left sides, at $x = 0$ and $x = a$, were impermeable and adiabatic. The theoretical and numerical model was used to obtain the transient two-dimensional temperature and moisture accumulation profiles in the solution domain subject to the above conditions.

The governing equations for the heat and mass transport process in a porous medium, subject to a steady forced convective airflow, were derived using the local volume averaging technique for the equations of mass, momentum, and energy transport (Kaviany 1991). Using this formulation, the local properties in the equations were averaged over a representative elementary volume, i.e. the smallest volume that represents the local average properties. In this derivation, two main assumptions are made: first, the thermal and mass transfer properties of porous medium

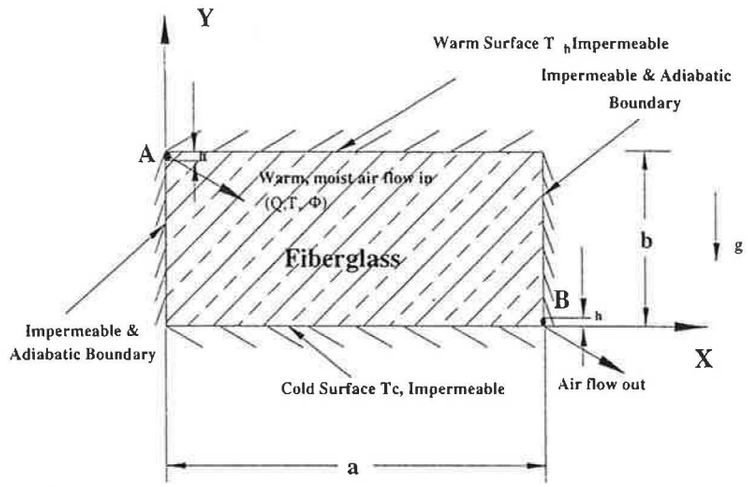

Figure 1. Schematic diagram for the model

are isotropic and homogeneous except for permeability; second, the porous system which consists of the solid, liquid, and gas phase is assumed to be in local thermodynamic equilibrium (i.e., all phases have the same temperature and pressure at any point). The assumptions implied for the use of volume average equations for heat and mass transfer in porous media are discussed in several sources (Whitaker 1977, Kaviany 1991).

Other assumptions were made to obtain the governing equations for the model developed here. These were:

1. The airflow through insulation is steady and forced and is two-dimensional with a glass-fiber pore-size Reynolds number ($Re_d < 1$) while buoyancy forces are negligible compared to the viscous forced convection; i.e., the Raleigh number for the porous medium is negligible (Nield and Bejan 1992).
2. With the small moisture content in the fiberglass insulation at the end of each experiment, it is assumed that liquid capillarity or liquid macroscopic velocity can be neglected. According to Ceagleske and Hovgen (1937) and Tien and Vafai (1990), for small amounts of liquid accumulation in the porous insulation (i.e., saturation values less than 0.1), the condensate will exist in a discontinuous pendular state, which means the liquid is essentially immobile.
3. Due to the low volume fraction of fiber in insulation material, and the low airflow velocity through the insulation (Reynolds number based on pore size < 1), thermal dispersion and mass dispersion can be neglected. Molecular diffusion of heat and water vapor, coupled with forced convection are the only means of transport within the gaseous component.
4. Compared with the heat conduction and convection, heat transfer effects by radiation are quite small and can be neglected, (Verschoor and Greeble 1952, Mumaw 1968, Lopez 1969).
5. The thermal and transport properties of each individual phase in the porous medium are either dependent on temperature or constant.
6. No chemical reactions take place in the fiberglass insulation during the experimental process.
7. When the local relative humidity reaches 100% at a location in the fiberglass insulation, ablimation, or water vapor solidification as frost on the glass fibers, is considered if the local temperature is below 0°C, and condensation is considered if the local temperature is above 0°C. No subcooling of liquid droplets is included because the phase change is primarily

between water vapor and either its liquid or solid phase, not between the liquid and solid phase of water.

8. The insulation structure is rigid and does not change shape during testing.
9. In the frozen region, the frost does not exist as a porous media except on the cold plate where a frost growth model is coupled to the numerical domain.
10. Additional assumptions for the properties and initial and boundary conditions are presented with the corresponding equations. The governing equations, based on the local volume average technique and all the assumptions mentioned above are presented below while the symbols are defined in the Nomenclature

The gas phase momentum equation (Darcy's law) is:

$$U = -\frac{K_x}{\mu}\frac{\partial P_g}{\partial y} \tag{1}$$

$$V = -\frac{K_y}{\mu}\frac{\partial P_g}{\partial y} \tag{2}$$

where K = permeability of the porous media (fiberglass) due to gas flow. Since the insulation slab was layered, the permeability may differ depending on whether the flow is parallel to the insulation layer (K_x) or normal to the layers (K_y).

The thermal energy equation for steady state pressure and negligible kinetic energy at every point is:

$$\frac{\partial(\rho c_p T)}{\partial t} + \frac{\partial(\rho_g c_{pg} UT)}{\partial x} + \frac{\partial(\rho_g c_{pg} VT)}{\partial y} + \Delta i \cdot \dot{n} = \frac{\partial}{\partial x}\left(k_{eff}\frac{\partial T}{\partial x}\right) + \frac{\partial}{\partial y}\left(k_{eff}\frac{\partial T}{\partial y}\right) \tag{3}$$

where
$$\rho = (1-\varepsilon)\rho_\sigma + \varepsilon_\beta \rho_\beta + \varepsilon_g \rho_g \tag{4}$$

$$c_p = [(1-\varepsilon)(\rho c_p)_\sigma + \varepsilon_\beta(\rho c_p)_\beta + \varepsilon_g \rho_g c_{pg}] / \rho \tag{5}$$

and
$$k_{eff} = \varepsilon_\beta k_\beta + \varepsilon_g k_g + k_\sigma(1-\varepsilon) \tag{6}$$

The water vapor convection and diffusion equation is:

$$\frac{\partial(\varepsilon_g \rho_{cg})}{\partial t} + \frac{\partial(\rho_{cg} U)}{\partial x} + \frac{\partial(\rho_{cg} V)}{\partial y} = \frac{\partial}{\partial x}\left[\rho_g D_{eff}^{cg}\frac{\partial}{\partial x}\left(\frac{\rho_{cg}}{\rho_g}\right)\right] + \frac{\partial}{\partial x}\left[\rho_g D_{eff}^{cg}\frac{\partial}{\partial y}\left(\frac{\rho_{cg}}{\rho_g}\right)\right] + \dot{n} \tag{7}$$

where D_{eff}^{cg} is assumed to be:

$$D_{eff}^{cg} = \varepsilon_g D/\tau \tag{8}$$

The liquid or solid ice phase continuity equation is:

$$\frac{\partial \varepsilon_\beta}{\partial t} + \frac{\dot{n}}{\rho_\beta} = 0 \tag{9}$$

The accompanying thermodynamic relations are:

$$p_{cg} = \rho_{cg} R_{cg} T \tag{10}$$

$$p_{ng} = \rho_{ng} R_{ng} T \tag{11}$$

$$p_g = p_{cg} + p_{ng} \tag{12}$$

$$\rho_g = \rho_{cg} + \rho_{ng} \tag{13}$$

The Clapeyron equation, for saturation conditions, is taken to be

$$p_{cg} = p_{cg}^0 \exp\left[-\frac{\Delta i}{16 R_{cg}}\left(\frac{1}{T} - \frac{1}{T_0}\right)\right] \tag{14}$$

In the above set of equations, the momentum effects can be reduced to the relatively simple Darcy Equations (1) and (2). The justification for this is that the pore-size Reynolds number was small for all the cases studied here (i.e. $10^{-6} < \mathrm{Re}_d < 10^{-5}$). At the same time, buoyancy forces were neglected because viscous forced convection dominated. The argument for this can be presented using dimensionless numbers for the conditions investigated. The Archimedes number Ar_b, or the ratio of buoyancy to inertial forces, was of order 10^{-4} or less; while the Reynolds number Re_b, based on the flow height of the porous slab, which is the ratio of inertial to viscous forces, was of order 50. This implies the ratio of buoyancy to viscous forces, $\mathrm{Ar}_b\mathrm{Re}_b$, is less than 10^{-2} or 1% everywhere for the test conditions investigated. For the highly porous fiberglass insulation (i.e. $\varepsilon \approx 0.98$), irreversible thermodynamic coupling between heat and mass transfer effects were not included because these coupling effects have not been measured for such materials.

Adsorption was included in the model by using the heat of adsorption for Δi in Equation (3) as measured by Tao et al. (1993) and the mass of adsorption from the adsorption isotherm presented by Simonson et al. (1993).

Initial and Boundary Conditions

For the air exfiltration simulations, the entire fiberglass insulation was initially at a uniform temperature (room temperature), with the liquid volume fraction near zero (dry), a uniform gas density throughout the insulation, and with the rate of phase change and water vapor density set to zero.

For air exfiltration, the inlet airflow rate, temperature and water vapor density are known values or can be calculated from the known property data. Boundary conditions for the warm surface and two insulated side walls can be set easily. For the insulated side walls, heat flux and mass flux were set to zero except for the inlet. For the top warm side, mass flux was set to zero and the temperature was constant.

Because a layer of frost grows on the bottom cold plate, the boundary conditions on the cold plate are more complex than an impermeable plate at a specified temperature. A frost growth model, developed by Tao et al. (1991b) and presented in Appendix A, was used to obtain the boundary conditions for temperature and water vapor partial pressure. From this frost growth model, a frost surface temperature was obtained as a boundary condition of the energy Equation (3) and then Clapeyron's Equation (14) was used to calculate the water vapor density at the frost surface as a boundary condition for the vapor transfer Equation (7). The thickness of the frost

growing on the cold plate δ_f was estimated to be less than 2% of the total height of the insulation b (i.e. $\delta_f << b$). Therefore, it was assumed that frost growth did not change the domain size for Equations (1) to (14). It should be noted that the introduction of the frost growth model as a boundary condition of the cold side causes this boundary condition to become nonlinear, resulting in some new difficulties for the numerical solution of the governing equations. The boundary conditions on the cold side of the numerical domain are:

$$T|_{y=0}(x,t) = T_{fs}(x,t) \qquad (0 \le x \le a) \tag{15}$$

$$p_{cg}|_{y=0}(x,t) = p^0_{cg} \exp\left[-\frac{\Delta i}{R_{cg}}\left(\frac{1}{T_{fs}(x,t)} - \frac{1}{T_0}\right)\right] \qquad (0 \le x \le a) \tag{16}$$

where the frost-air interface temperature $T_{fs}(x,t)$ was obtained from the frost growth model (Appendix A).

The validity of this frost growth model boundary condition was investigated in a simulation study for the test facility investigated here. Although the temperature profiles obtained by using the frost growth model on the cold plate were almost the same as those obtained from the simple constant temperature and the impermeable boundary conditions on the cold plate, the moisture accumulation was significantly different. The difference between the moisture accumulated in the bottom layer as calculated using these two different boundary conditions was about 20%, with the frost growth model consistently giving larger frost accumulation rates.

Method of Solution

Momentum Equations (1) and (2) are considered to be independent of other equations, which means that, the airflow field or streamlines are not affected by heat and mass transfer. Generally, this is true when the pore-size Peclet number < 1 (Nield and Bejan 1992). Separating the momentum equation from the other equations greatly simplifies the solution of the problem defined by Equation (3) to (14).

From momentum Equations (1) and (2), we could obtain

$$\frac{\partial U}{\partial x} = -\frac{K_x}{\mu}\frac{\partial^2 P}{\partial x^2} \tag{17}$$

$$\frac{\partial V}{\partial y} = -\frac{K_y}{\mu}\frac{\partial^2 P}{\partial y^2} \tag{18}$$

Adding Equations (17) and (18), and assuming incompressible flow, gives,

$$\frac{\partial^2 P}{\partial x'^2} + \frac{\partial^2 P}{\partial y^2} = 0 \tag{19}$$

where the x coordinate is transformed by the equation

$$x = x'\sqrt{\frac{K_x}{K_y}} \tag{20}$$

Errors in the velocity field resulting from changes in density have been as large as 1%, due to both the pressure gradient in the porous insulation and condensation and ablimation of water vapor but density changes due to cooling were larger. The experimental data shows that density

changes due to cooling were less than 10% for the top four layers of insulation, and less than 15% for all layers. The sensitivity of the temperature and moisture accumulation profiles to changes in flow is investigated in more detail in Part II.

Equation (19) is Laplace's equation, and the theoretical solution (Milne-Thompson 1968) is available for sources or sinks on one surface between two parallel plates, a geometry similar to the problem considered here. Using the results of Milne-Thompson's derivation for the (x',y) space, the solutions for the pressure can be obtained for the (x',y) space and, thereafter, the velocity profile can be obtained by using Equations (17) and (18).

Equations (17) to (19) allow us to decouple the fluid flow problem from the heat and water vapor transfer problems. The momentum Equations (1) and (2) were solved independently of the other Equations (3) to (16). Among the remaining equations, the energy and vapor transfer equations are nonlinear, coupled, and partial differential equations. These equations can only be solved numerically based on their discretized forms. The Control Volume Formulation (Patankar 1980) was used to obtain the finite difference forms of the governing equations. Once the finite difference equations had been established, they were solved by an iterative "line by line" method (Patankar 1980). The dimensions of the insulation slab (calculation domain) were 600 mm wide by 135 mm high, and this was modeled using 40 × 46 = 1840 control volumes. Grids of a higher density were put near the cold side (i.e. a non-uniform grid in y direction), because the temperature and moisture accumulation distributions in the y direction near the cold side were of greatest interest. It was found that further refining the grid i.e. increasing the numbers of grid points and decreasing the grid spacing did not affect the simulation results. For example, increasing the number of grids by 30% changed the results less than 0.5%. The time step size used for all the simulations was 5 s. Decreasing this time step by 50% changed the results less than 1% but doubled the computing time. Therefore, the simulation results can be considered as insensitive to the grid spacing and time step.

EXPERIMENTAL APPARATUS AND PROCEDURE

Figure 2 is a schematic of the experimental test cell section, which is 600 mm wide, 135 mm high and 275 mm deep. Moist warm air was introduced at the inlet slot located in the left-top

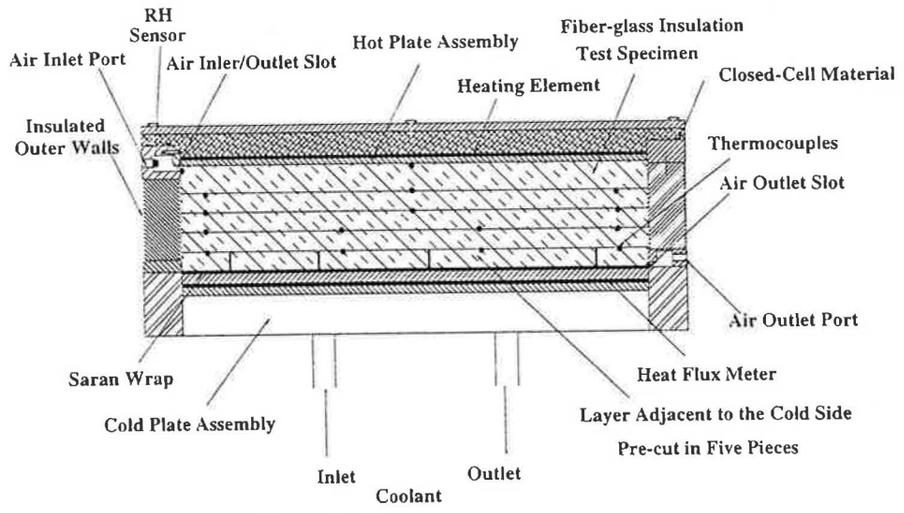

Figure 2. Cross-sectional view of test cell

corner, and was removed at the outlet slot located in the right-bottom corner. A five layer, medium-density (50 kg/m^3), glass-fiber slab with a total dimension of 275 mm by 600 mm by 135 mm was placed in the test section for each test. This test slab geometry is perhaps somewhat similar to the geometry of some building envelope components with air entering at room temperature as exfiltration at one crack and exiting the cold side. This simple two-dimensional geometry allows us to obtain test data for the insulation alone, without the complication of coupling effects with other components, buoyancy and three-dimensional effects that frequently occur in building envelopes.

A cold plate, which could be cooled to a temperature of −20°C by a heat exchanger, was placed at the bottom of the test section. An electrically heated plate was placed on the top of the test section to keep the temperature near 21.5°C. It was found, both in the numerical simulations and experiments, that electrical power to heat the top plate was not required during the exfiltration tests to keep the hot-plate at 21.5°C because the heat conduction gain from the top surface during the test was negligible.

A calibrated heat-flux meter (uncertainty ±4.0 W/m^2) was mounted within the cold plate to measure the heat flux through the cold plate assembly during each test. Thirty-eight thermocouples (type T, calibration uncertainty ±0.2°C) were located between the fiberglass layers and at the inlet/outlet slots and cold plate heat-flux meter.

A calibrated relative humidity sensor (uncertainty 2% rh) was located in the left-top corner air inlet slot. This sensor was used to ensure that the humidity of the airflow during the exfiltration tests remained constant. To start a test, the volumetric airflow rate is set using a mass flow controller with an uncertainty of 0.8% of the full range rate (20 L/min).

During each test, data from the flow meter sensor, the relative humidity sensor, temperature sensors in the fiberglass insulation and cold plate heat-flux meter, the airflow temperature at the inlet and outlet, and the temperature of the hot plate were sampled every 60 s and recorded.

The moisture accumulation in each sample insulation layer was measured at the end of each test by weighing each sample prior to (oven dry condition) and at the end of each experiment. Considering the repeatability of the two identical experiments, the measurement uncertainty was within 1% moisture content by dry mass. It was found both numerically and experimentally that the moisture accumulation within the insulation layer adjacent to the cold side is much larger than in other layers. Therefore, only this layer is precut in five pieces in order to obtain the moisture accumulation profile along the x-direction. The size of the five pieces was chosen in order to expect nearly the same accuracies for each piece when measuring the mass of moisture accumulation. A layer of polyethylene wrap was located on the cold plate for collecting the frost growing on the cold plate and used to pull the bottom layer of insulation out of the test cell at the end of each test. The mass of the frost on the polyethylene and within the insulation slab was calculated as part of the moisture accumulation within the insulation layer adjacent to the cold side.

Parameters and Apparatus for Air Exfiltration Test

Although a typical indoor relative humidity during cold periods of winter rarely exceeds 50% rh and values of 20% rh are common in most buildings, the exfiltration tests were conducted with room temperature air at a high relative humidity (60% to 84%). These high relative humidities were used in order to obtain experimental data over a reasonably short testing period with small relative errors so that the numerical model could be validated with a higher degree of accuracy. For the air exfiltration experiment, the inlet air relative humidity values were set to be 60%, 70%, and 84%, with the inlet air temperature maintained at 21.5°C. The hot plate was kept at 21.5°C (±1°C) and the cold plate temperature is kept at −20°C (±1°C). During each test, the variations in the supply air temperature were less than 0.5°C. Variations in supply air temperature from one replication test to another were slightly larger (i.e. ±1°C).

Table 1. Parameters Used in the Exfiltration Tests

Test No.	Inlet Flow Rate Q, L/min	Inlet Flow Relative Humidity, %	Test Period t, hours
1	10	84	2.5
2	10	84	3.5
3	10	70	3.5
4	10	60	3.5
5	5	84	3.5
6	5	60	3.5
7	15	77	3.5
8	15	60	3.5

Cold plate temperature T_C = −20°C, hot plate temperature T_h = 21.5°C, and inlet air temperature T_{in} = 21.5°C

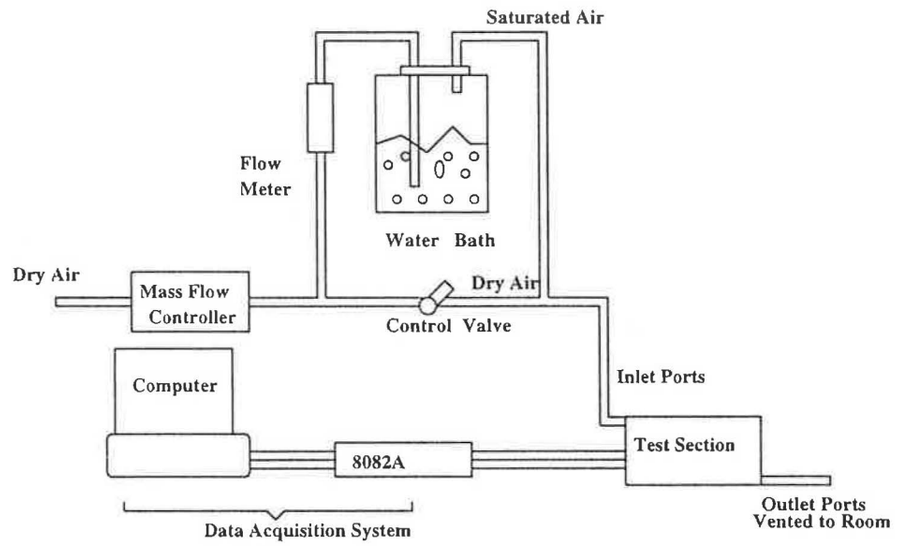

Figure 3. Apparatus

The range of airflow rates used in this study was based partly on a field investigation by Shaw et al. (1987). His investigation found that a typical detached Canadian residential house experiences an average air exfiltration rate of 0.98 L/(m^2·s). The range of data for infiltration/exfiltration is very large, from very tight houses to very leaky houses. In a study of air leakage through walls of an apartment block, the measured leakage was greater than 1.0 L/(m^2·s) for a 10 Pa pressure difference (Shaw et al. 1991). In our study it was convenient to select high exfiltration rates because they reduced the duration of tests and relative experimental errors in the moisture accumulation measurements. For the current test section dimension (275 mm by 600 mm by 135 mm), flow rates for the experiment were selected to be 5 L/min, 10 L/min, and 15 L/min. Without considering any density changes, the corresponding surface air exfiltration rates were 0.5, 1.0, and 1.5 L/(m^2·s) and the air speeds at the center of test section (i.e., in the x direction) were 2.24 mm/s, 4.49 mm/s, and 6.73 mm/s, respectively. The air inlet flow conditions for each test are listed in the Table 1.

The apparatus for controlling the airflow and humidity during the exfiltration tests is shown in Figure 3. Compressed air first passes through an industrial dryer, and then flows through the

mass flow controller at the selected total airflow. In generating the required range of inlet relative humidity (60% to 84%), a water bath was implemented. By adjusting the airflow using a flow meter and a control valve, a portion of the dry air was diverted from the main line to the bottom of the water bath. As the air moved up through the bath, it became very humid (80% to 100% rh depending on flow rate). By mixing this humid air with dry air in the correct proportions, the desired air relative humidity was obtained. The mixed air was introduced into the left-top portion of the test section shown in Figure 2 through six inlet ports. For an airflow of 15 L/min, the maximum relative humidity obtained was 77%.

Properties of the Insulation Samples

The insulation samples used in the test cell were commercially available 25 mm thick medium density fiberglass boards. Except for the top board, which was 38 mm thick, these were purchased in single bundles to eliminate property variations that may occur during different manufacturing runs. Although the 275 mm by 600 mm boards tested had a dry density range of 49.5 to 50.6 kg/m^3, the variation in density within individual boards ranged from a high of 52.9 kg/m^3 to a low of 41.4 kg/m^3. That is, in each board there are regions of density that are both higher and lower than the board average. These regions of significant density variation in each board typically had a length scale that was approximately equal to the board thickness or about 25 mm. When the insulation boards were placed in the test cell and compressed slightly by the lid, any region of low density is compressed more than those of high density, which causes the density to become more uniform throughout the test cell. When averaged over the depth of the test cell (275 mm) density variations are expected to be insignificant. For the numerical studies a uniform dry density 50 kg/m^3 was used throughout the domain of integration.

The airflow streamlines within a porous medium like fiberglass with a Darcy flow depend on the air viscosity μ and permeability K, as implied by Equations (1) and (2) was uniform but not isotropic. As noted previously, the air viscosity depends only on its absolute temperature. Although the permeability can vary nonuniformly from place to place within the test cell as a result of variations in local insulation density, when averaged over the depth of the test call (275 mm), variations in both the density and the uniformity of the permeability were expected to be insignificant.

The permeability of layered insulation materials may differ with airflow direction. These nonisotropic permeability coefficients for fiberglass boards were investigated for Darcy type airflow normal to the board surface and parallel to its surface. To measure the differences in these two permeabilities, K_x and K_y, the test cell was filled with insulation boards (135 mm by 550 mm by 275 mm). In one case their orientation was normal to the bottom surface and, later, parallel to the bottom surface. These two cases ensured isothermal airflow air and had a Darcy velocity parallel to the bottom surface. Each permeability, K_x and K_y, was calculated using Equation (1) in the form

$$K = \frac{U_0 \mu L}{\Delta P} \tag{21}$$

where $L = 0.55$ m, giving $K_y = (1.28 \pm 0.05) \times 10^{-9}$ m^2 and $K_x = (2.16 \pm 0.09) \times 10^{-9}$ m^2. Thus for a given pressure difference the Darcy velocity was 40% lower in the y than in the x direction. The importance of this non-isotropic permeability will be illustrated in detail in the numerical results presented in Part II.

The thermal conductivity k_{eff} used for the fiberglass boards, could show directional characteristics as well as nonuniformities within the test cell. Since the apparent thermal conductivity of dry samples of fiberglass were shown to be a function of fiber diameter and orientation, density

and absolute temperature (ASHRAE 1993), the potential for variations in k_{eff} with position and orientation needs investigation. In the same manner, as permeability and spatial variations in insulation density throughout the test cell were expected to be small when the density was averaged over the depth of the test cell (275 mm). Spatial variations in the absolute temperature were not insignificant and could have resulted in a special variation in the apparent thermal conductivity of up to 6% about the mean value (A sensitivity study for k_{eff} is included in part II).

The directional characteristics of k_{eff} were investigated in a separate study. The apparent thermal conductivity of the fiberglass boards ($k_{eff\text{-}x}$ and $k_{eff\text{-}y}$) was measured in the test cell for dry samples of boards orientated both parallel to the bottom and top surface using the following equation:

$$k_{eff} = \frac{q'' b}{A \Delta T} \tag{22}$$

giving $k_{eff\text{-}x} = 0.034 \pm 0.002$ and $k_{eff\text{-}y} = 0.035 \pm 0.002$ W/(m·K)

Because the difference between $k_{eff\text{-}x}$ and $k_{eff\text{-}y}$ was small and within the experimental uncertainty, the apparent thermal conductivity of a dry sample was taken to be a constant in the numerical model with a value of 0.034 W/(m·K) (thermal conductivity sensitivity is investigated in Part II).

Test Procedure

The following is an outline of the test procedure used for each experiment.

1. Before each test, the insulation samples (four boards and five small pieces) were dried by placing all of them in an oven at 110°C for about 14 hours. After this, the insulation samples were removed from the oven, wrapped in cling-wrap polyethylene film, and cooled to room temperature for about 4 hours. At that time, the insulation samples were considered to be totally dry, with the liquid volume fraction equal to zero. After cooling to room temperature, each insulation sample, within its polyethylene wrap, is then weighed on the digital scale.
2. A layer of polyethylene wrap was carefully put on the surface of cold plate. Each of the five pieces of insulation which form the layer of insulation adjacent to the cold plate in experiments was unwrapped from its polyethylene wrap and placed on the cold plate in correct order. Four thermocouples were then positioned on the top of this layer at selected locations. Two very-thin, one-inch wide nylon straps were then put on the top of this layer in order to aid in the removal of the top four upper layers after each test.
3. Another insulation board was then unwrapped and pressed down to the top of bottom layer, and another four thermocouples are positioned at the selected positions. This process was repeated until all the layers and thermocouples were in place.
4. The hot plate (lid) was put in place and fastened with the six fastening screws to seal the test cell so that the flow only entered at the top inlet port and exited at the outlet port. The data acquisition system was started, and the ethylene glycol-water mixture pumped to the cold plate, the mass flow controller was then opened to start the flow of air into the test section, thereby commencing the test. During the test, all the data recorded were recorded on a hard disk for further analysis. The wrappings for insulation samples were individually weighed so that the actual dry weight of each insulation sample could be calculated.
5. The mass flow controller and the pump supplying the cooling fluid to the cold plate were turned off at the end of each test. The lid covering the test section was removed, and the top four layers of insulation were lifted by two nylon strips. These top four layers were then wrapped inside their original wrappings. The layer formed by five individual pieces of insulation adjacent to the cold plate and the frost accumulation just under this layer were lifted by the

layer of polyethylene wrap which was put on the cold plate in step 2, and covered the front and back walls of the test section. A very sharp blade was now used to cut this layer of polyethylene wrap along the boundaries of each insulation piece so that each piece of sample could be separated along with the frost accumulated under it on the polyethylene wrap. The five pieces of insulation board sample and five pieces of polyethylene wrap were then wrapped in their original wrappings.

6. All the wrapped samples were weighed. The five pieces of polyethylene wrap containing the frost accumulation in the bottom layer were then dried at room temperature for about 4 hours, and then weighed individually to calculate the actual frost accumulation in each piece adjacent to cold plate.

The numerical and experimental results and model validation will be shown in part II.

SUMMARY AND CONCLUSIONS

Part I of this paper presents the basic equations and describes the experimental test facility used to investigate the heat transfer and moisture and frost accumulation in an insulated cavity subjected to cold environmental temperatures while humid warm air flowed through the cavity in a two-dimensional flow pattern from the warm side to the cold side. The assumptions used in the model were discussed in the light of the experimental test conditions. Special attention was given to the development of an accurate frost growth model on the cold plate because a large fraction of the frost accumulated on this surface.

The properties of the fiberglass insulation boards used in the tests were evaluated in independent tests. It was found that although there are variations in density within each board, these were expected to be insignificant when averaged over the depth of the test cell. The variations in permeability normal (K_y) and parallel (K_x) to the plane of each board were significant and were taken into account for the flow calculation. Dry samples of the fiberglass boards were found to have apparent isotropic thermal conductivity properties.

Test conditions were selected for the test facility that would allow the collection of accurate data over a reasonably short time, which can be compared to the simulation results. These comparisons are made in Part II.

APPENDIX A

Frost Growth Model On The Cold Plate

In this study, it was found that, after some time, a dense layer of frost was formed on the cold plate. Due to this layer of frost, the boundary condition at $y = 0$ was more complex than an impermeable plate at a specified temperature. Proper boundary conditions at the cold side of a fibrous matrix need to be developed for heat and mass transfer modeling because a large portion of the frost was found to accumulate on the cold plate. A one-dimensional frost growth model (Tao et al. 1991) was applied to give these boundary conditions.

Many studies on frost growth on solid surfaces under convection conditions have been conducted (O'Neal and Tree 1985). Most of them used a lumped model, i.e., an average frost density normal to the cold plate, due to the lack of experimental data on spatial variation of the frost density. The frost model chosen also used the concept of the average frost density in the y direction. This means that the frost porosity, $\varepsilon_f = \rho_f/\rho_{ice}$, is the same throughout the frost layer in the y direction.

A schematic of the insulation slab with frost on the cold plate boundary is shown in Figure A1. Δx is element of length in the x direction of a control volume used for solving the numerical model. Since Δx is much smaller than a, it can be assumed that the frost surface temperature T_{fs},

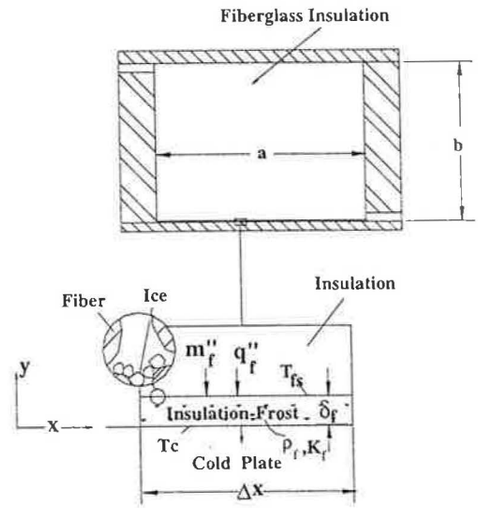

Figure A1. Configuration of Frost Growth Model

frost thickness δ_f, frost density ρ_f, frost layer effective thermal conductivity k_f, heat flux into the frost layer $\dot{q}''$, and vapor diffusion flux into the frost layer $\dot{m}''$, changed discontinuously from node to node in x direction. Over the range of one node element Δx, the transfer of water vapor takes place only at $y = \delta f$.

The mass balance applied to the frost layer interface, which forms on the cold plate and grows into the fibrous matrix, yields,

$$m''_f = \varepsilon\left(\delta_f \frac{d\rho_f}{dt} + \rho_f \frac{d\delta_f}{dt}\right) \tag{A1}$$

where $\varepsilon = 1 - \varepsilon_\sigma$ is the porosity of the insulation slab in the dry condition and $\varepsilon\delta_f\rho_f$ is the mass of frost in the frost layer. The densification of the frost layer, shown in Figure A1, obeys the following mass diffusion equation:

$$\delta \frac{d\rho_f}{dt} = -D\left(\frac{1 - \rho_f/\rho_{ice}}{\tau_f}\right)\left.\frac{d\rho_v}{dT}\right|_s \frac{T_{fs} - T_c}{\delta_f} \tag{A2}$$

where the right hand side of the equation describes the molecular diffusion of water vapor within the frost layer and τ_f is the tortuosity in the frost layer. Considering the presence of glass fibers in the frost layer, τ_f is chosen as $\tau_f = 1.2$ in calculation ($\tau_f = 1.1$ is often used for the frost layer growing on the solid surface under convection without glass fibers). $(d\rho_v/dT)|_s$ can be obtained using the Clapeyron Equation.

$$\left.\frac{d\rho_v}{dT}\right|_s = \exp\left[-\frac{\Delta i}{R_v}\left(\frac{1}{T_{fs}} - \frac{1}{T_{ref}}\right)\right]\frac{\Delta i}{R_v T_{fs}^2} \tag{A3}$$

An energy balance at the frost-layer-insulation interface *fs* gives the heat flux

$$\dot{q}_f'' = k_f \frac{T_{fs} - T_c}{\delta_f} - \Delta i \dot{m}_f'' \tag{A4}$$

Equation (A5) includes the frost layer thermal conductivity k_f, which must take into consideration the contribution of the glass fiber thermal conductivity k_σ and the volume fraction of ice in the frost layer, $\varepsilon_\beta = \varepsilon\varepsilon_f = \varepsilon(\rho_f/\rho_{ice})$ as well as conduction in the air and water vapor contained inside the frost layer

$$k_f = \varepsilon_\sigma k_\sigma + \varepsilon_\beta k_\beta + \varepsilon_\gamma \frac{k_v \rho_v + k_a \rho_a}{\rho_v + \rho_a} \tag{A5}$$

Equations (A1) through (A5) describe this frost growth model. Together they give a complete description of the average frost density ρ_f, the thickness of the insulation-frost domain δ_f, and the temperature at the boundary between the insulation domain and the insulation-frost layer domain T_{fs}. Simulation studies show that T_{fs} is less than 1 K warmer than the cold plate for the conditions investigated.

The frost growth model only provides the boundary conditions for energy and vapor transport equations and does not change the calculation domain within the insulation because δ_f is much smaller than the total insulation height b (e.g., $\delta_f/b < 0.01$). Therefore heat flux and mass flux into the frost layer can be calculated using following equations for the properties above the frost layer

$$\dot{q}_f'' = -k_{eff} \left.\frac{\partial T}{\partial y}\right|_{y=0} \tag{A6}$$

$$\dot{m}_f'' = -D_{eff} \left.\frac{\partial \rho_v}{\partial y}\right|_{y=0} \tag{A7}$$

Equations (A1) through (A7) are to be used with all governing equations previously introduced.

The solution method for the frost growth model can be described with the following steps.

1. Assume a frost surface temperature T_{fs}, as the boundary condition for the energy Equation (3); and, by using the Clapeyron Equation, the frost surface vapor density is obtained for the boundary condition of vapor transfer Equation (7).
2. Solve energy Equation (3) and vapor transfer Equation (7) based on the assumed boundary conditions
3. Calculate the heat flux into the frost layer $\dot{q}_f''$ and the vapor diffusion flux into the frost layer $\dot{m}_f''$ by using Equations (A6) and (A7)
4. Solve Equation (A1) to (A4) based on the calculated value of $\dot{q}_f''$ and $\dot{m}_f''$ and obtain an update value of T_{fs}.
5. Repeat steps 1 through 3 until converged solutions are obtained.

Numerically, when the local relative humidity of a control volume adjacent to the cold plate reaches 100%, the frost growth model is used for that control volume as a boundary condition. Small values, 0.1 kg/m^3 and 10^{-4} m, are used as initial conditions for the frost density and frost thickness in the frost growth model. Before the relative humidity of a control volume adjacent to the cold plate reaches 100%, the cold plate boundary is as an impermeable one, with a specified temperature T_c.

NOMENCLATURE

A	cross-sectional area of insulation slab, m^2
Ar_b	Archimedes number based on height of porous slab, $\mathrm{Ar}_b = \mathrm{Ra}_b/\mathrm{Pe}_b\mathrm{Re}_b$
a	width of test porous slab, m
b	height of test porous slab, m
c_p	heat capacity at constant pressure, J/(kg·K)
D	molecular diffusivity of water vapor, m^2/s
d	glass-fiber diameter, m
g	gravity, m/s^2
h	width of inlet slot, m
K	permeability, m^2
k	thermal conductivity, W/(m·K)
L	length of the insulation slab in permeability test, m
$\dot{m}''$	mass flux kg/(m^2·s)
$\dot{n}$	rate of phase change, kg/(m^3·s)
P	pressure, Pa
Pe_b	Peclet number based on height of porous slab, $\mathrm{Pe}_b = U_0 b/a$
$\dot{q}''$	heat flux, W/m^2
R	gas constant, J/(kg·K)
Ra_b	Raleigh number based on slab height, $g\rho\Delta T b^3/\mu T$
Re_d	Reynolds number based on pore size, $\mathrm{Re}_d = \rho u d/\mu$
Re_b	Reynolds number based on height of porous slab, $\mathrm{Re}_b = \rho u b/\mu$
rh	relative humidity
T	temperature, K
T_c	cold-plate temperature, K
T_{fs}	frost surface temperature, K
T_h	hot-plate temperature, K
t	time, s
U	x direction velocity, m/s
U_0	uniform velocity in center of test section, m/s
V	y direction velocity, m/s
x, y	coordinate axes, m
μ	viscosity, kg/(m·s)
ρ	density, kg/m^3
α	thermal diffusivity, m^2/s
ε	porosity of insulation material
τ	tortuosity
ϕ	relative humidity
δ_f	frost layer thickness, m
ΔP	pressure difference, Pa
ΔT	temperature difference, K
Δi	enthalpy of phase change, J/kg

Subscripts

eff	effective properties
cg	condensable gas
f	frost
fs	frost surface
g	gas phase (air and vapor)
ng	noncondensable
v	vapor
x	x direction
y	y direction
β	liquid or ice phase
σ	solid phase

Superscripts

cg	condensable gas
0	reference value

REFERENCES

ASHRAE. 1993. *ASHRAE Handbook—Fundamentals*, SI Edition. Atlanta: ASHRAE.

Bomberg, M., and C. Shirtliffe. 1978. Influence of Moisture and Moisture Gradients on Heat Transfer through Porous Building Materials. ASTM STP 660: 211-33.

Bomberg, M., et al. 1991. Moisture Research in North America: 25 Years of Building Science. Lund, Sweden: Lund University.

Ceagleske, N.H., and O.A. Hougen. 1937. Drying of Granular Solids. *Ind. Eng. Chem.* 29: 805-813.

CIB. 1993. *Proc. CIB* International Symposium on Moisture Problems in Building Walls. Rotterdam, The Netherlands: CIB.

CIB. 1995. *Proc.* International Symposium on Moisture Problems in Building Walls. Rotterdam, The Netherlands: CIB.

Epstein, K.A. and L.E. Putnam. 1977. Performance Criteria for the Protected Membrane Roof System. In *Proceedings* of the Symposium on Roofing Technology, sponsored by the National Bureau of standards National Roofing Contractors Association.

Graves, R.S., and D.C. Wysocki. 1991. Insulation Materials, Testing and Applications. ASTM STP 1116.

Hedlin, C.P. 1983. Effect of Moisture on Thermal Resistances of Some Insulation in a Flat Roof System under Field-Type Conditions. ASTM STP 789: 602-25.

International Energy Agency (IEA). 1995. Annex 24 *Final Report* Vols. 1-3. Heat, Air and Moisture Transfer Through New and Retrofitted Insulated Envelope Parts (Hamtie). Laboratorium Bouwfysica, Department Burgerlijke Bouwkunde, Univ. Louvain. Leuven Belgium.

Kaviany, M. 1991. *Principles of Heat Transfer in Porous Media.* New York: Springer-Verlag Inc.

Kohonen R., and T. Ojanen. 1987. Non-Steady-State Coupled Diffusion and Convection Heat and Mass Transfer in Porous Media. In *Proc.* 5th International Conference on Numerical Methods in Thermal Problems, Montreal, Canada 5(1): 705-716.

Kumaran, M.K. 1992. Heat, Air and Moisture Transport Through Building Materials and Components: Can we calculate and predict? In *Proc.* Sixth Conference on Building Science and Technology, pp. 129-144. University of Waterloo: ON. Canada

Langlais, C., M. Hyrien, and S. Klarsfeld. 1983. Influence of Moisture on Heat Transfer through Fibrous Insulating Materials. ASTM STP 789: 563-81.

Larsson, L.E., J. Ondrus, and B.A. Petersson. 1977. The Protected Membrane Roof (PMR)—A Study Combining Field and Laboratory Tests. In *Proc.* Symposium on Roofing Technology, NBS and NRCA. NIST

Lopez, E.L. 1969. Techniques for Improving the Thermal Performance of Low-Density Fibrous Insulation. Prog. Astronaut. Aeronaut. 23: 153-172.

Lstiburek, J., and J. Carmody. 1990. *Moisture Control Handbook.* ORNL/Sub/89-SD 350/1. Oak Ridge, TN: Oak Ridge National Laboratory.

Milne-Thompson, L.M. 1968. *Theoretical Hydrodynamics*, 5th ed. London: Macmillan.

Mitchell, D.R., Y.-X. Tao, and R.W. Besant. 1995. Air Filtration with Moisture and Frosting Phase Changes in Fiberglass Insulation: I Experiment, II Model Validation. *Int. J. Heat Mass Transfer* 38(9): 1587-1596, and 1597-1605.

Mumaw, J.R. 1968. Variations of the Thermal Conductivity Coefficient for Fibrous Insulation Materials. M.S. Thesis, The Ohio State University, Columbus. OH.

Murata, Keiji. 1995. Heat and Mass Transfer with Condensation in a Fibrous Insulation Slab Bounded on One Side by a Cold Surface. *Int. J. of Heat and Mass Transfer* 38 (17): 3253-3262.

Nield, D.A., and A. Bejan. 1992. *Convection in Porous Media.* New York: Springer-Verlag, Inc.

Ojanen, T., and C. Simonson. 1995. Convective Moisture Accumulation in Structures with Additional Inside Insulation. In *Proc.* Thermal Performance of the Exterior Envelopes of Buildings VI, ASHRAE/DOE/BETEC/ORNL Conference, Dec. 4.-8. pp. 745-752. Atlanta: ASHRAE.

O'Neal, D.L., and D.R. Tree. 1985. A Review of Frost Formation in Simple Geometries. *ASHRAE Transactions* 91 (2):267-281.

Paljak, I. 1973. Condensation in Slabs of Cellular Plastics. *Materiaux et Constructions* 6(31):53.

Patankar, S.V. 1980. *Numerical Heat Transfer and Fluid Flow.* New York: Hemisphere.

Pedersen, C.R. 1990. Combined Heat and Moisture Transfer in Building Construction. *Report No.* 214, Thermal Insulation Laboratory, Technical University of Denmark, Lyngby, Denmark.

Pedersen, C.R., T.W. Petrie, G.E. Courville, P.W. Childs, and K.E. Wikes. 1991. Moisture Migration and Drying Rates for Low Slope Roof—Preliminary Results. In *Proc.* 3rd International Symposium on Roofing Technology. NRCA, Rosemont, IL.

Pierce, D.A., and S.M. Benner.1986. Thermally Induced Hygroscopic Mass Transfer in Fibrous Medium. *Int. J. Heat Mass Transfer* 29: 1683-1694.

Shaw, C.Y. 1987. Methods for Estimating Air Exchange Rates and Sizing Mechanical Ventilation System for Houses. *ASHRAE Transactions* 93 (2) 2284-2302.

Shaw, C.Y., R.J. Magee, and J. Rousseau. 1991. Overall and Component Airtightness Values of Five-Story Apartment building. *ASHRAE Transactions* 97(2): 347-353.

Simonson, C.J., Y-X Tao, and R.W. Besant. 1993. Thermal Hysteresis in Porous Insulation. *Int. J. Heat Mass Transfer* 36:4287-4297.

Tao, Y-X, R.W. Besant, and K.S. Rezkallah. 1991a. Unsteady Heat and Mass Transfer with Phase Changes in an Insulation Slab: Frosting Effects. *Int. J. Heat Mass Transfer* 34:1593-1603.

Tao, Y-X, R.W. Besant, and K.S. Rezkallah. 1991b. Modeling of Frost Formation in a Fibrous Insulation Slab and on an Adjacent Cold Plate. *Int. Comm. Heat Mass Transfer* 18: 609-618.

Tao, Y-X, R.W. Besant, and C.J. Simonson. 1993. Measurement of the Heat of Adsorption for a Typical Fibrous Insulation. *ASHRAE Transactions* 98(2):495-501.

Tien, H.C., and K. Vafai. 1990. A Synthesis of Infiltration Effects on an Insulation Matrix. *Int. J. Heat Mass Transfer* 33: 1263-1280.

Thomas, W.C., G.P. Bal, and R.J. Onega. 1983. Heat and Moisture Transfer in Glass Fiber Roof-Insulating Material. ASTM STP 789: 582-601.

Tobiasson, W., and J. Richard. 1977. Moisture Gain and its Thermal Consequence for Common Roof Insulation. In *Proceedings* 5th Conference on Roofing Technology, NBS and NRCA, Chicago, IL.

Trechsel, H.R. 1994. *Moisture Control in Buildings.* ASTM Manual Series: MNL 18. W. Conshohoken, PA: ASTM.

Vafai, K., and S. Sarker. 1986. Condensation Effects in a Fibrous Insulation Slab. *J. Heat Transfer* 108, 667-675.

Vafai, K., and H.C. Tien. 1989. A Numerical Investigation of Phase Change Effects in Porous Materials. *J. Heat Transfer* 33: 1263-1280.

Verschoor, J.D., and P. Greeble. 1952. Heat Transfer by Gas Conduction and Radiation in Fibrous insulation. *Trans. ASME* 74: 961-968.

Whitaker, S. 1977. Simultaneous Heat, Mass and Momentum Transfer in Porous Media: A Theory of Drying. Advances in Heat Transfer Vol. 13: 119-203.